Identifying suitable digital elevation models and deriving features for landslide assessment in Idukki District, Kerala, India

A. Shameem Ansar[1,*], S. Sudha[1] and Suresh Francis[2]

[1]Department of Electrical and Electronics Engineering, National Institute of Technology, Tiruchirappalli 620 015, India
[2]Kerala State Remote Sensing and Environment Centre, Thiruvananthapuram 695 033, India

This study compares the vertical accuracy of different digital elevation models (DEMs), such as Cartosat-I, ASTER-GDEM, SRTM-GL1, ALOS3D30 and FABDEM with a resolution of 30 m, to the toposheet-derived 264 spot heights of Idukki district, Kerala, India, obtained from the Survey of India. We quantitatively assess the vertical accuracy of these DEMs by analysing their accuracy against randomly selected topographic map spot heights. The study also validates the accuracy of the DEMs by evaluating the vertical accuracy separately for different elevation classes representing varying terrain characteristics of the Idukki district. Statistical measures are used to evaluate the performance of the DEMs. The results of the study show that FABDEM exhibits an RMSE of 41.79 m, which is lower than that of other models. The study utilizes FABDEM to derive a set of 12 geomorphological and hydrogeological features, including slope, aspect, elevation, profile curvature, plan curvature, distance to road, relative relief, ruggedness index, drainage density, height above near drainage, wetness index and stream power index. The characteristics of various parameters are analysed. The uniqueness of this study lies in its utilization of geomorphological and hydrogeological features derived from FABDEM that directly impact the susceptibility of landslides in the region. The study identifies that a combination of these dynamic and static parameters, which vary with elevation classes, plays a significant role in determining landslide occurrence in this region.

Keywords: Digital elevation models, geomorphological and hydrogeological features, landslide, spot height, vertical accuracy.

DIGITAL Elevation Models (DEMs) are digital representations of the bare ground topographic surface of the earth, excluding trees, buildings and other surface objects. DEMs are created from a variety of sources, including topographic maps, and are commonly used in various applications such as Geographic Information Systems (GIS)[1]. DEM provides accurate information necessary for various applications such as GIS and often replaces topographical maps to derive the main causative factors such as slope, aspect, elevation, distance to road, drainage density, curvature, etc. It can be also used for analysis of hydrological modelling, landforms, viewshed and in modelling mass movements like landslides. The accuracy of DEMs is crucial as errors in DEMs can propagate during data processing, affecting the quality of the output of the applications in which they are used[2]. Therefore, it is important to assess the accuracy of DEMs before applying them to geographical analysis. The importance of DEMs in geographical applications has led to the generation of different implementable models with wide range of use cases. A thorough analysis of nearly 200 studies has been conducted earlier to evaluate the methods used for assessing DEM accuracy over the past three decades[3]. The accuracy of DEMs can be evaluated using various sources such as topographic maps, Shuttle Radar Topography Mission (SRTM) DEM, Advanced Spaceborne Thermal Emission and Reflection Radiometer (ASTER), Global Digital Elevation Model (GDEM), and stereo-pair aerial photographs[4]. These evaluations ensure the usability of DEMs in diverse applications related to topography and earth sciences.

The generation of multiple DEMs with diverse characteristics provides opportunities for improving the accuracy and reliability of geographical applications. Using DEMs with different resolutions, accuracies or data sources, researchers can account for uncertainties and limitations in the data and obtain a more comprehensive understanding of the studied phenomena. Furthermore, the availability of free global DEMs improves the accessibility and use of these data in various applications. However, it is important to consider the limitations and potential errors associated with different DEMs and carefully select and evaluate the ones appropriate for specific requirements.

Table 1 summarizes previous studies conducted in India on assessing elevation accuracy using the root mean square error (RMSE) of widely used DEMs[5–13]. DEM accuracy is highly influenced by various aspects of the terrain, including spatial resolution, elevation range, land-cover conditions and relief. Continuous improvement in the accuracy and availability of DEMs enables a more robust assessment of the accuracy of susceptibility maps[14]. The accuracy of a

*For correspondence. (e-mail: shameemansar@gmail.com)

Table 1. Summary of research works conducted in India on elevation accuracy assessment

Author details	Study area	Landcover and the number of reference points considered	Root mean square error of digital elevation model (DEM) used			
Mahesh *et al.*	Tamil Nadu	Creek, canal, beach, dune, grassland, casuarina plantation, barren land, mudflat and settlements (275)	AW3D30-V3-2.48 m SRTM-V3(30 m) – 3.02 m Carto-DEM V3R1-3.88 m ASTERGDEM V2-8.02 m			
Divya Sekhar Vaka *et al.*	Bihar, Katarniaght WL, Manali, Himachal Pradesh	Flat terrain with agriculture (1612) Flat terrain with forest cover (28) Snow-covered mountains (36)	TDX90 SRTM 90 NASADEM	Relative relief (m)		
				Bihar	KWLS	Manali
Mukherjee *et al.*	Western part of Shiwalik-Himalaya	Highly rugged terrain (31 GCPS)	Cartosat-1 – 4.83 m ASTER30 – 16.06 m SRTM30 – 18.91 m	1.43 5.34 2.06	5.88 6.82 5.25	13.11 17.15 7.41
Rawat *et al.*	Shahjahanpur district	Highly rugged terrain and significant variation of relief (20 GCPs)	Cartodem-ASTER – 137.65 m Cartodem-SRTM – 186.65 m ASTER-SRTM – 50.87 m			
Jain *et al.*	Lower Tapi Basin (3837 sq. km)	Narrow valley, hilly terrain, agricultural fields and coastal regions (117)	SRTM (30 m) – 2.88 ASTER-2 (30 m) – 5.4 Carto-DEM – 3.5 AW3D30 – 2.45			
Patel *et al.*	Maulana Azad National Institute of Technology (MANIT), Bhopal, Madhya Pradesh	Uneven topography with small hills (830)	Cartosat-1 (30 m) – 3.49 ASTER DEM (30 m) – 3.49 SRTM (90) – 3.72			
Mukherjee *et al.*	Shiwalik Himalaya	Rugged terrain with steep slopes, ridges and flat topography (11)	Cartosat-1 DEM – 3.14–7.24 m Varying with grid spacing from 10 to 150 m			
Rastogi *et al*.	Chandra and Bhaga basins, Himalayan	Chandra Basin – 2835 points Bhaga Basin – 2160 points	Cartosat-1 DEM – Chandra basin: 10.8 m Bhaga basin: 9 m			
Thomas *et al.*	(i) Muthirapuzha River Basin – (271.75 sq. km) (ii) Pambar and river basin (288.53 sq. km), Kerala	Hills and plateau (28)	ASTER-GDEM (30 m) SRTM (30 m) GMTED (30 m)	Relative relief (m) <200 21.8 10.4 36.5	 200–400 31.75 22.51 50.99	 >400 42.08 29.55 86.75

DEM is found to vary from a couple of metres to hundreds of metres. The accuracy is also observed to decrease in areas with steep terrain.

Only a few landslide susceptibility mapping studies have been conducted for the Idukki district, Kerala, India, which is regularly prone to landslides, using features generated from DEM. Susceptibility mapping was done using ASTER GDEM of 30 m resolution and ML algorithms[15,16]. Landslide factors such as slope, aspect, curvature, topographic wetness, stream power and topographic ruggedness were derived from the DEM. However, many other essential features influence landslides directly, and their inclusion would help develop a more accurate susceptibility model. Additionally, a study on impact of the landslide features using DEM with fairly low inaccuracy is required.

The freely available DEMs for the Idukki district, Kerala, have a resolution of 30 m. Due to the unavailability of high-resolution DEMs to the research community, globally available 30 m resolution DEMs are used in this study area. Therefore, when comparing the DEMs for Idukki, the accuracy is considered better, and toposheets are used as absolute values for comparison. The primary objective of this study is to identify the most accurate DEM with 30 m resolution for the Idukki district, Kerala. The DEM options considered for evaluation are Cartosat-1, ASTER GDEM, SRTMGL1, ALOS World 3D-30 m and forest and buildings removed Copernicus DEM (FABDEM). The chosen DEM will be utilized to derive geomorphological and hydrogeological features that directly impact the susceptibility of landslides in the study district.

Review of the study area

The Idukki district, Kerala, is characterized by its high-altitude plateau, which features rugged mountainous terrain, numerous river valleys and deep gorges. It covers an area of 4358 sq. km and is known for its varied topography and geomorphological features. As shown in Figure 1 the district is situated between 90°15′N and 100°21′N lat., 76°37′E and 77°25′E long. and is characterized by mountains and forests that encompass approximately 97% of its total area. The northern part of Idukki forms a sub-plateau that is higher in altitude compared to the rest of the district. The landform

begins at an elevation of 600 m amsl, with the maximum altitude reaching up to 2647 m, making it the highest point in South India and 13 other peaks standing at over 2000 m in height. However, the unique topography of the region also makes it highly vulnerable to landslides, with more than 3500 of them being reported in the past decade, according to the Geological Survey of India (GSI)[17]. Therefore, accurate geomorphological characterization derived from an accurate DEM is essential for building precise landslide-susceptibility mapping models to mitigate landslide risks in the region. The Idukki district is known for its varied topography and geomorphological features, including mountains, forests and steep altitudes. The complexity of terrain characteristics and its vulnerability to landslides warrants accurate DEM data for developing effective landslide susceptibility models for the region.

Data sources

Topographic map of the Idukki district, Kerala, from the open series map (OSM) of the Survey of India (SoI), and five DEMs, viz. Cartosat-1 V3, ASTER GDEM V3, SRTMGL1 V3, ALOS World 3D V3.2 and FABDEM version 1.0 were used in this study. SoI OSMs were obtained from the Kerala State Remote Sensing and Environment Centre (KSREC), Thiruvananthapuram. The geoportal Bhuvan of the National Remote Sensing Centre provided Cartosat-I DEM data. SRTMGL1 data was downloaded from the Earth Resource Observation and Science Centre (EROS) of USGS, ASTER data from the Terrestrial Remote Sensing Data Analysis Centre, and ALOS World 3D data from Open-Topography. FABDEM was obtained from Fathom Global, an environmental service company which provides flood mapping, risk analytics and insurance recovery service. The height system used by various data sources and in the present study was geoid; Earth Gravitational Model of 1996 (EGM96). It represents the equipotential surface of the Earth's gravity field that best fits the mean sea level. Within the framework of this study, landslide information collected from GSI and KSREC for the period 2007–20 was archived and geo-referenced on the ArcGIS platform. Discrete point data were identified to provide geographical locations and validated according to reports and maps of landslide history. Based on the available data, landslides had occurred in the Idukki district, Kerala, at 3973 locations. These are represented in Figure 2.

Topographic map

Topography is a decisive factor in the functioning of various natural processes. The topographic map of a region represents ground relief, forest cover, drainage, populated areas,

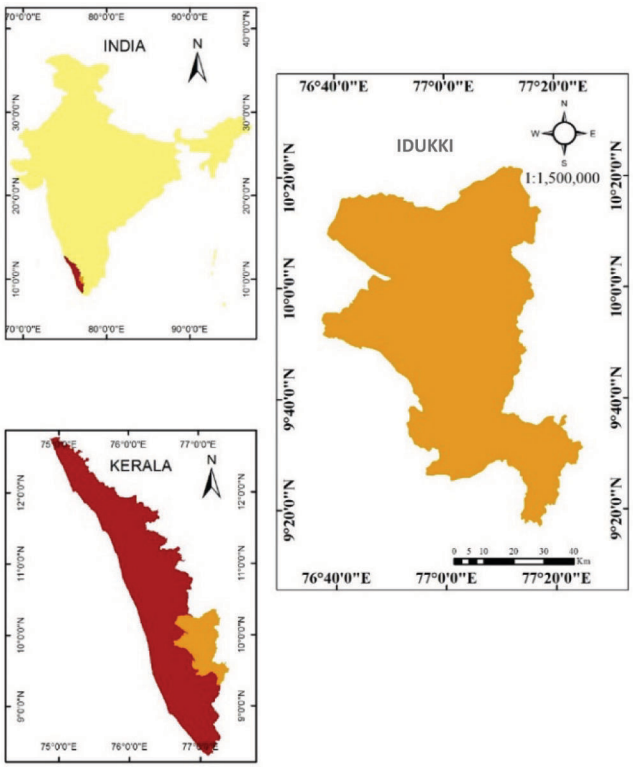

Figure 1. Location map of the study area, Idukki district, Kerala, India.

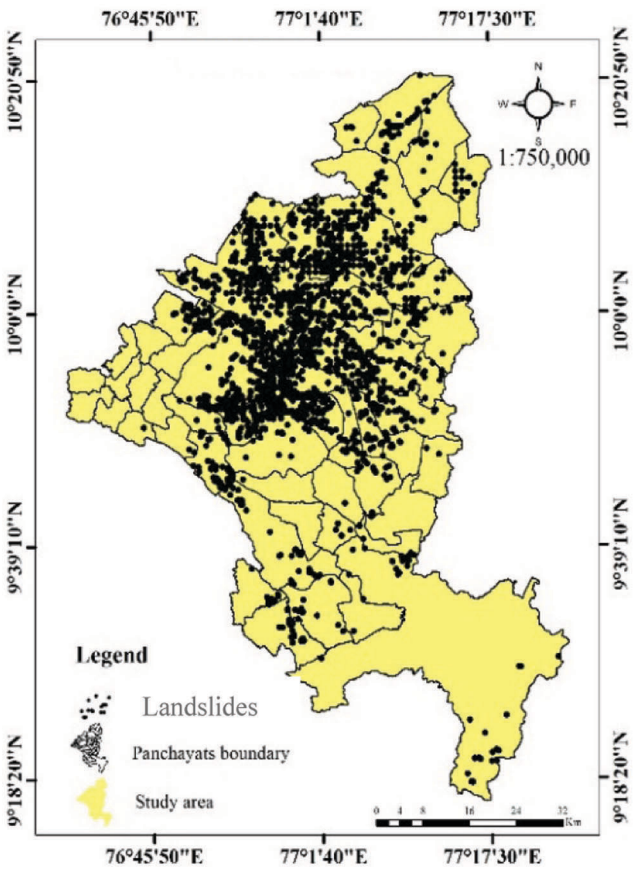

Figure 2. Location of landslides in Idukki district, Kerala.

Table 2. Characteristics of DEMs

DEM characteristics	Cartosat-I DEM	ASTER-GDEM	NASA SRTMGL1	AW3D30	FABDEM
Release year	2005	2019	2015	2021	2020
Version	V3	V3 R1	V3	V3.2	V1-0
Data format	GeoTIFF	GeoTIFF	GeoTIFF	GeoTIFF	GeoTIFF
Coordinate system	GCS_WGS_1984	GCS_WGS_1984	GCS_WGS_1984	GCS_WGS_1984	GCS_WGS_1984
Satellite	Cartosat-1	Terra	Space shuttle endeavour	Advanced land observing satellite	Sentinel-1
Resolution	1 arcsec (30 m)	1 arcsec (30 m)	1 arcsec (30 m)	1 arcsec (30 m)	1 arcsec (30 m)
Geographic projection	Latitude, Longitude	Latitude, Longitude	Latitude, Longitude	Latitude, Longitude	Latitude, Longitude
Datum	WGS_1984 (H) EGM96 (V)	WGS_1984 (H) EGM96 (V)	WGS_1984 (H) EGM96 (V)	WGS_1984 (H) EGM96 (V)	WGS_1984 (H) EGM96 (V)
Data sources	http://bhuvan.nrsc.gov.in	https://earthexplorer.usgs.gov/	https://earthexplorer.usgs.gov/	https://www.eorc.jaxa.jp/ALOS/en/index_e.htm	https://www.fathom.global/product/fabdem/
Last accessed	15 January 2022	20 March 2022	20 March 2022	8 April 2022	April 2023

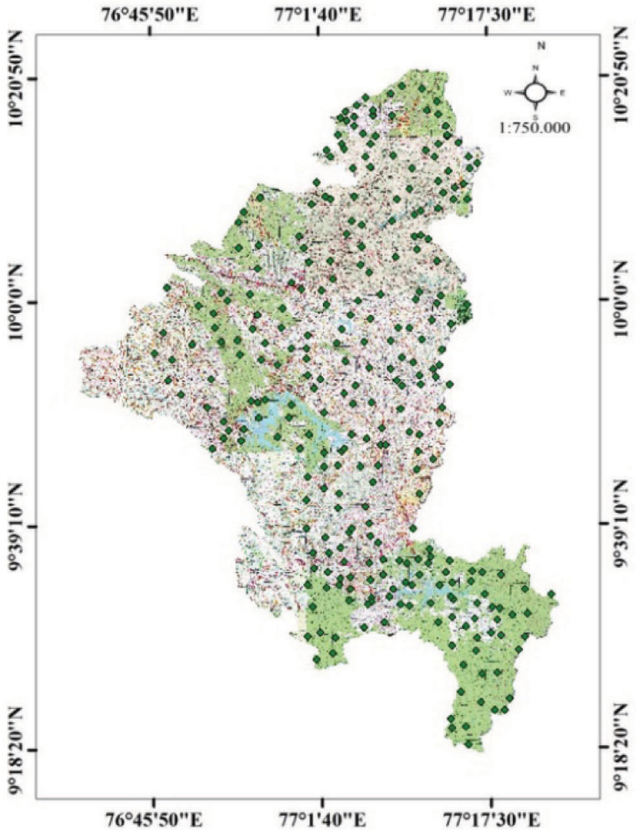

Figure 3. Spot height points on the topographical map.

transportation routes, artificial features, etc. It, therefore, requires quantitative analysis and correction to determine the relative effectiveness of its constituents and operating mechanisms[18]. The contour lines with equal elevation points help depict the shape and elevation of the land. This map represents the three-dimensional undulating terrain on a two-dimensional surface with universal transverse mercator (UTM) projection and World Geodetic System 1984 (WGS84) datum. The vertical datum is the mean sea level as defined by EGM96. The topographic map of Idukki comprises 14 different sheets of OSM of SoI, namely C43K16, C43Q9, C43Q13, C43Q14, C43Q15, C43L3, C43L4, C43L8, C43R1, C43R2, C43R3, C43R5, C43R6 and C43R7, in 1 : 50,000 scale with 20m contour interval.

Digital elevation models

DEMS help extract topographical parameters to analyse the overall shape of the Earth's surface. DEM forms a regular matrix representation of the continuous variation of relief over space and is a digital model of the Earth's surface. It provides information about the elevation or relief of a terrain. The registration process of DEMs is crucial as it enables the seamless integration of a DEM with other geospatial datasets. This integration allows for various applications, including terrain analysis, hydrological modelling, visualization, mapping, etc. This can be achieved using surface matching algorithms and the iterative closest point (ICP) algorithm[19]. These methods involve finding corresponding points or features in multiple DEMs and aligning them for a consistent representation of the terrain.

The DEMs used here include Cartosat-1 V3, ASTER-GDEM V3, SRTM-GL1 V3, ALOS world 3D V3.2 and FABDEM V1.0. All the DEMs and the toposheets used have been co-registered and are in the UTM Zone 43 N projection and WGS 84 datum. Table 2 lists the characteristics of these DEMs[20–26].

Methodology

This study aims to identify the most accurate DEM and then extract landslide-influencing factors from it. Identification of the accurate DEM is a two-step process that involves: (i) the selection of points from the same points of spot heights and DEMs and (ii) the evaluation of DEMs. Points selected were identical for spot heights and DEMs, and care was taken to identify open locations. Ground observations from the SoI OSM provide positional information with reference data. Randomly specific topographic points

Table 3. Statistical measures

Statistical measure	Equation	Description
Error (X_e)	$(X_i - X_t)$	Provides elevation difference
Mean (μ)	$\mu = 1/n \sum_{i=1}^{n} X_i$	It is the average of the samples
Standard deviation (SD)	$\mathrm{SD} = \sqrt{\frac{\sum (X_i - \mu)^2}{n-1}}$	It shows the distribution of values across a given dataset
Mean bias error (MBE)	$\mathrm{MBE} = 1/n \sum_{i=1}^{n} (X_i - X_t)$	Bias ($X_i - X_t$) is defined as the estimate of systematic error. The positive values indicate overestimation and negative values indicate underestimation of actual values (X_t)
Mean absolute error (MAE)	$\mathrm{MAE} = 1/n \sum_{i=1}^{n} \lvert(X_i - X_t)\rvert$	It is the average of the absolute values of the errors ($X_i - X_t$), thereby indicating the average magnitude of the errors
Root mean square error (RMSE)	$\mathrm{RMSE} = \sqrt{1/n \sum_{i=1}^{n} (X_i - X_t)^2}$	This is a commonly used measure of the difference between values DEMs and observed values over the reference

X_i, DEM elevation corresponding to the reference point; X_t, Elevation corresponding to the same reference point of the toposheet. RMSE is mainly used to verify how close the estimates are to the actual topographic height. This is used as a measure of DEM assessment, and lower the RMSE, better is the accuracy. The DEM with minimal error is chosen as the most accurate model.

were chosen and compared with their respective elevation in DEM to determine the model accuracy. This process was performed for all DEMs. The Geoid height system in this study represents the equipotential surface of the Earth's gravity field that best fits the mean sea level. This ensures a consistent reference surface for elevation measurements. To benchmark, it is required to bring all datasets to the exact WGS-1984 horizontal and EGM96 vertical datum. Hence, Cartosat-1 data were converted into EGM96 using Geospatial Data Abstraction Library (GDAL) utilities. The steps involved in the proposed methodology are outlined below.

Random points selection

Publically available OSMs of SoI were used in this study. Spot heights for various locations were selected from the OSMs. Two hundred and sixty-four random points of the topographical map were obtained as reference data. These are marked as spot heights in Figure 3. The Idukki district, Kerala, showcases a wide range of topography, encompassing high-altitude plateaus, rugged mountainous terrain, numerous river valleys, deep gorges and forested regions. The landform of the district begins at an elevation of 600 m amsl. The DEM accuracy generally decreases from the plains to the hilly terrain, which warrants elevation classification in the comparison of DEMs. Moreover, the geographical features of the district were studied in terms of landslide susceptibility, with historical data indicating an increase in landslide susceptibility with the increase in elevation. As a result, the accuracy of DEM assessment is based on various elevation categories to account for the presence of these distinctive geographical features. As a result, the accuracy of DEM assessment is based on various elevation categories to account for the presence of these distinctive geographical features. The spot height points were categorized into four different regions based on contour elevation, namely (a) low-elevation area (1–782 m), (b) moderate elevation area (783–1330 m), (c) high elevation area (1331–1910 m) and (d) very high elevation area (1911–2637 m) for comparison of accuracies across elevations. Digitization converts the geographical data from scanned images to vector data by plotting the characteristics as a point layer on ArcGIS, and features of the plotted map are captured as point coordinates.

Evaluation of DEM accuracy

For all DEMs, elevation corresponding to the 264 topographic reference points was extracted using interpolated resampling methods through the elevation analysis service of ArcGIS. For each of the extracted values, various statistical measures such as mean (μ), standard deviation (SD), mean bias error (MBE), mean absolute error (MAE) and root mean square error (RMSE) were determined to evaluate the DEMs (Table 3)[27,28].

Feature derivation

Based on the knowledge of the domain expert, features that influence landslides were derived from the highly accurate DEM. The DEM features were classified into two groups, namely geomorphological and hydrogeological features. This included 12 features, viz. slope angle, aspect, elevation, profile curvature, plan curvature, distance to road, relative relief, terrain ruggedness index (TRI) drainage

density, height above near drainage (HAND), topographic wetness index (TWI) and stream power index (SPI).

Slope angle is an essential geomorphological factor determining shear forces, shear stresses and saturation levels[29]. The aspect of the slope, defined by its azimuth, has multifaceted effects on the exposure to sunlight, precipitation impacts, weathering processes, soil characteristics, canopy development and root growth. These interrelated factors collectively shape the ecological dynamics and environmental conditions of the slope, showcasing the complex interplay between topography, climate and ecosystem development[30,31]. Elevation is also a significant factor in landslides because the high and undulating surface results in a steep slope that is reliable for slope instability. The curvature of a hill serves as a valuable indicator of its inherent shape and has profound implications for understanding landslide dynamics. By recognizing the connection between curvature, water accumulation, soil stability and triggering events, researchers and practitioners can take proactive measures to mitigate landslide risks and ensure safer land use practices. Profile curvature measures the surface curve in one slope direction and enhances the erosion and deposition process. In contrast, plan curvature in a horizontal plane influences the convergence or divergence of water during run-off. Two factors, namely drainage density and HAND, were used to determine the effect of the river[32]. SPI and TWI are the most critical hydrological factors predicting the susceptibility of landslides. SPI indicates erosion and discharge power in a specific area as represented in eq. (1).

$$\mathrm{SPI} = A_s * \tan(\beta), \tag{1}$$

where A_s is a specific catchment area and β is the slope angle (°).

TWI is utilized to evaluate and communicate specific hydrological characteristics within a given geographical area. In the context of hydrology and environmental science, TWI is particularly employed to assess moisture content, groundwater conditions and surface flow accumulation within a watershed or landscape. This quantitative parameter is calculated using eq. (2).

$$\mathrm{TWI} = \ln\left(\frac{\alpha}{\tan(\beta)}\right), \tag{2}$$

where α is the cumulative ascending drainage zone across a point and β is the slope angle (degrees) at the point.

With respect to human activities, the most crucial factor is 'distance to road'. Constructing roads on steep slopes could lead to the elimination of foundational support from the lower terrain. Modifying the slope and increasing the steepness of a region increases the risk of slope failure[33]. The drainage system combines slope, lithology and topography extracted from the DEM to determine the drainage density.

Results

The performance of the DEMs was examined based on vertical accuracy. The features were derived from the accurate DEM, and the landslide points were assessed. A detailed discussion is presented below.

Performance of the DEMs

The elevation corresponding to the 264 randomly selected points on the topographic map was generated separately for each DEM. The maximum elevation of 2637 m in reference data corresponded to 2512, 2548, 2587, 2621 and 2625 m of Cartosat-I, ASTER-GDEM, SRTM-GL1, AW3D30 and FABDEM respectively. Figure 4 shows the elevation error for all 264 points of all DEMs.

From the figure, the error is found to increase with elevation. Table 4 lists the statistical measures for all 264 points. MBE of FABDEM outperforms the others in assessing systematic errors in estimation compared to a reference. A lower MAE value of FABDEM indicates greater model accuracy. RMSE of FABDEM is 41.79 m, followed by AW3D30, SRTMGL1 ASTER-GDEM and Cartosat-1. The low RMSE of FABDEM indicates that the values generated are close to the reference data showing better model accuracy.

Based on the elevation category, a total of 11 spot height points in low elevation area, 160 points in moderate elevation, 47 points in high elevation and 46 points in very high elevation area were identified and mapped to DEM. The area corresponding to each peak was obtained, and a similar procedure was followed for all DEMs. Figure 5 shows the elevation maps of FABDEM corresponding to four different elevation categories. Table 5 lists the statistical measures for these categories.

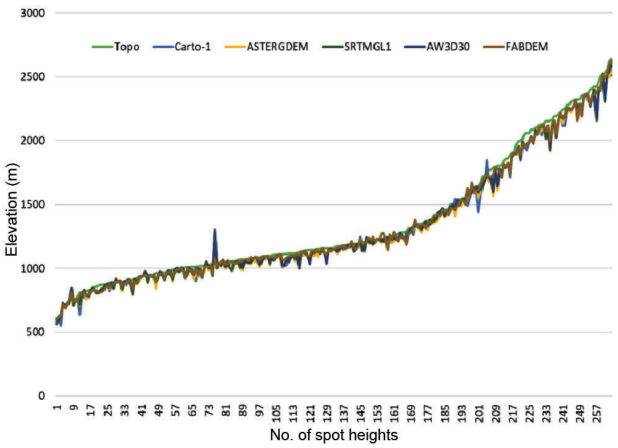

Figure 4. Elevations at different spot heights.

Table 4. Statistical comparison between topographical map spot heights and DEMs

Parameters	TopoMap	Cartosat-1	ASTER-GDEM	SRTM-GL1	AW3D30	FABDEM
Mean	1307.88	1317.27	1312.11	1319.03	1326	1329
SD	525.20	471.32	472.8	476.13	475.05	478.61
MBE		–35.3	–40.24	–33.65	–27	–24
MAE		40.7	43.74	37.58	31.34	28.02
RMSE		62.57	61.25	57.31	52.05	41.79

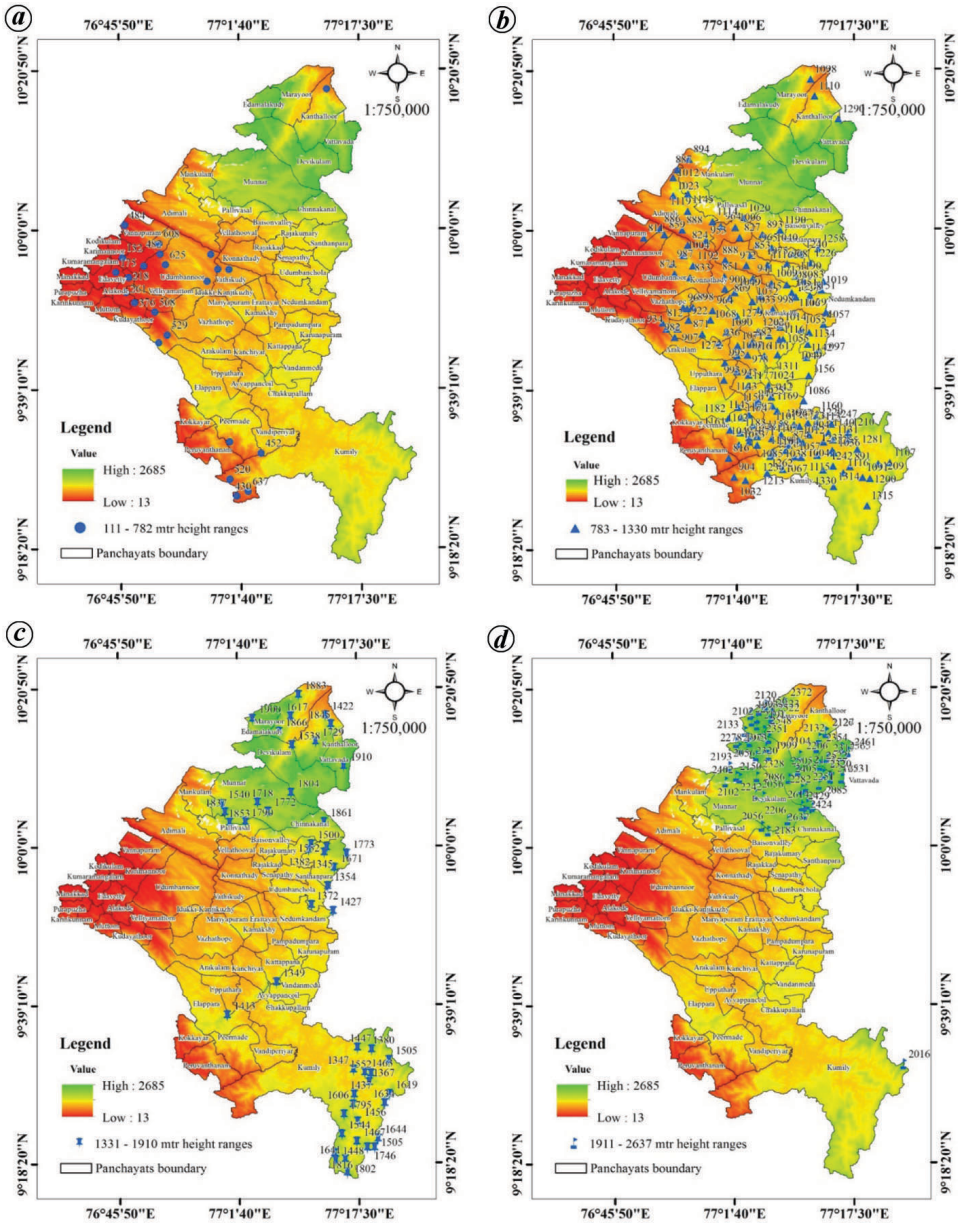

Figure 5. Elevation map of FABDEM for (***a***) low, (***b***) moderate, (***c***) high and (***d***) very high elevation areas.

Among the elevation categories of DEMs, FABDEM showed lower MAE and RMSE. RMSE increased from a low to a high value with the increase in elevation. RMSE value of low, moderate, high and very high elevation regions of FABDEM was 24.81, 29.53, 40.82 and 71.69 m respectively. The lower RMSE value of FABDEM for all elevations validates its overall vertical accuracy. The characteristics of the terrain being modelled could explain the increase in RMSE with increasing elevation.

Table 5. Statistical comparison of low, moderate, high and very high regions of topographical map reference spot heights and DEM elevations

Parameters	TopoMap	Cartosat-1	ASTER-GDEM	SRTM-GL1	AW2D30	FABDEM
Low elevation area (600–782 m)						
Mean	522.91	698.65	696.82	697.8	709	707
SD	215.43	83.3	73.50	76.25	73.87	65.5
MBE		–5.2	–6.12	–5.9	–0.45	–1.29
MAE		12.24	12.45	12.5	10.04	7.5
RMSE		37.62	32.92	35.07	33.81	24.81
Moderate elevation area (783–1330 m)						
Mean	1067.01	1043.49	1036.96	1041.79	1049	1050
SD	128.05	134.25	130.28	134.01	130.67	133.35
MBE		–23.5	–30.05	–25.22	–18.04	–16.41
MAE		29.86	35.12	30.9	24.50	21.77
RMSE		44.69	45.46	44.19	38.87	29.53
High elevation area (1331–1910 m)						
Mean	1598.21	1554.19	1545.82	1557.76	1566	1570
SD	179.08	168.16	171.32	165.30	165.25	171.14
MBE		–44.01	–52.38	–40.44	–31.85	–27.85
MAE		50.45	52.38	40.78	32.70	31.38
RMSE		69.79	67.49	55.13	50.77	40.82
Very high elevation area (1911–2637 m)						
Mean	2258.58	2175.37	2177.5	2187.95	2194	2202
SD	174.73	181.18	177.07	182.57	182.89	188.9
MBE		–83.21	–81.08	–70.63	–64.78	–56.91
MAE		83.31	81.30	70.63	64.86	57
RMSE		101.03	97.12	93.01	85.93	71.69

Feature derivation

The geomorphological and hydrogeological features of Idukki were extracted from FABDEM and classified into different classes (Figure 6 *a–l*). Table 6 shows the distribution and percentage of surface existence of each class over different features.

From Table 6, the following inferences can be made:

(i) The slope classes vary from very gentle to very steep slopes (Figure 6 *a*). Moderate and steep slopes collectively cover 23.19% and 34.7% respectively, of the total area.

(ii) Due to the topography of the study region, the elevation feature is divided into ten different classes (Figure 6 *c*). These classes have a minimum height of 20 m and a maximum height of 2660 m.

(iii) Aspect classes aid in the estimation of solar lighting for each location of the study region. The aspect feature of the Idukki district, Kerala, is classified into eight groups (Figure 6 *b*).

(iv) Plan curvature affects the erosion and downward motion of water flow and is classified into five classes (Figure 6 *d*). Among the distribution area, the convex region covers more than 80% of the surface.

(v) Profile curvature relates to the convergence and divergence of flow across a surface. As shown in Figure 6 *e*, profile curvature is grouped into five classes. Majority of the area is covered by the concave curvature class.

(vi) The effect of topography on the location of saturated sources of surplus production is represented by TWI (Figure 6 *f*). Among the five classes, more than 70% of the area is covered with 'low' index values.

(vii) TRI is a measurement of topographic heterogeneity (Figure 6 *j*). It is grouped into five classes, i.e. from very low to very high, with values between 0 and 1. More than 60% is spread across with moderate and high index values.

(viii) Road construction necessitates the extraction of materials from lower slopes that display attributes reminiscent of potential destabilization. Nine classes represent 'distance to road' (Figure 6 *g*). It is found that short-distance classes cover more than 70% of the surface area.

(ix) The relative relief provides the real change in altitude in a unit area relative to its local base level. Figure 6 *h* depicts the seven classes of relative relief. Also, 30.24% of the surface area has relative relief between 850 m and 1050 m.

(x) Figure 6 *i* represents five different classes of drainage density. More than 60% of the surface area is covered by a 'low' drainage density class (4–7 km/sq. km).

(xi) The HAND feature represents the vertical distance between a location and its nearest stream. The HAND classes are grouped into five (Figure 6 *k*). The low HAND classes are spread over most of the zone, collectively covering more than 80%.

(xii) SPI provides potential stream flow erosion at a given point. As represented in Figure 6 *l*, SPI is grouped into five classes varying from very low to very high. The major part of the area is covered by moderate, high and low SPI classes.

Table 6. Class distribution and percentage of surface existence over different features

Features	Class values	Distribution area (sq. km)	Percentage of surface existence	Class label
Slope (°)	0–8	750.69	17.19	Very gentle
	8–15	1,083.08	24.80	Gentle
	15–21	1,012.59	23.19	Moderate
	21–27	824.64	18.85	Moderate steep
	27–36	537.13	12.30	Steep
	36–75	157.7	3.60	Very steep
Aspect (°)	East (67.5–112.5)	320.05	7.3	
	North (0–22.5)	586.23	13.3	
	North (337.5–360)	442.91	10.14	
	Northeast (22.5–67.5)	461.74	10.58	
	Northwest (292.5–337.5)	583.48	13.3	
	South (157.5–202.5)	665.82	15.25	
	Southeast (112.5–157.5)	498.39	11.4	
	Southwest (202.5–247.5)	480.6	10.99	
	West (247.5–292.5)	266.85	6.11	
Profile curvature	–26 to –1.5	2.25	0.0005	High negative
	–1.5 to –0.43	34.67	0.80	Negative
	–0.43 to 0.2	217.32	4.97	Close to zero
	0.2 to 1.9	762.88	17.47	Positive
	1.9 to 27	3,348.72	76.70	High positive
TWI	<5.0	1,777.41	40.71	Very low
	5.0–7.0	1,658.61	38	Low
	7.0–9.0	577.48	13.22	Moderate
	9.0–13.0	237.19	5.43	High
	>13.0	115.15	2.63	Very high
TRI	<0.3	128.72	2.9	Very low
	0.3–0.4	869.23	19.59	Low
	0.4–0.5	1,500.26	33.82	Moderate
	0.5–0.6	1,337.00	30.13	High
	>0.6	600.79	13.55	Very high
Distance to road (m)	<1000	1,878.16	43.02	
	1,000–2,000	1,225.80	28.07	
	2,000–3,000	550.28	12.6	
	3,000–4,000	295.76	6.8	
	4,000–5,000	163.20	3.7	
	5,000–6,000	117.68	2.7	
	6,000–7,000	76.28	1.74	
	7,000–8,000	41.68	0.95	
	>8000	6.92	0.38	
Relative relief (m)	<250	360.35	8.25	
	250–450	1,061.16	24.3	
	450–650	423.13	9.6	
	650–850	828.44	18.97	
	850–1,050	1,320.7	30.24	
	1,050–1,250	218.76	5.01	
	1,250–1,450	152.46	3.49	
Drainage density (km/sq. km)	0.5–4	803.63	18.41	Very low
	4–7	2,717.82	62.26	Low
	7–11	748.99	17.16	Moderate
	11–14	82.36	1.89	High
	14–17	12.48	0.28	Very high
HAND (km/sq. km)	0–50	2,292.38	53.2	Very low
	50.1–100	1,208.65	28.05	Low
	100.1–200	543.55	12.61	Moderate
	200.1–400	209.01	4.86	High
	>400	54.96	1.27	Very high
SPI	<400	423.42	9.7	Very low
	400–7,500	858.11	19.65	Low
	7,500–25,000	1,429.97	32.75	Moderate
	25,000–55,000	1,280.22	29.3	High
	>55,000	374.12	8.6	Very high

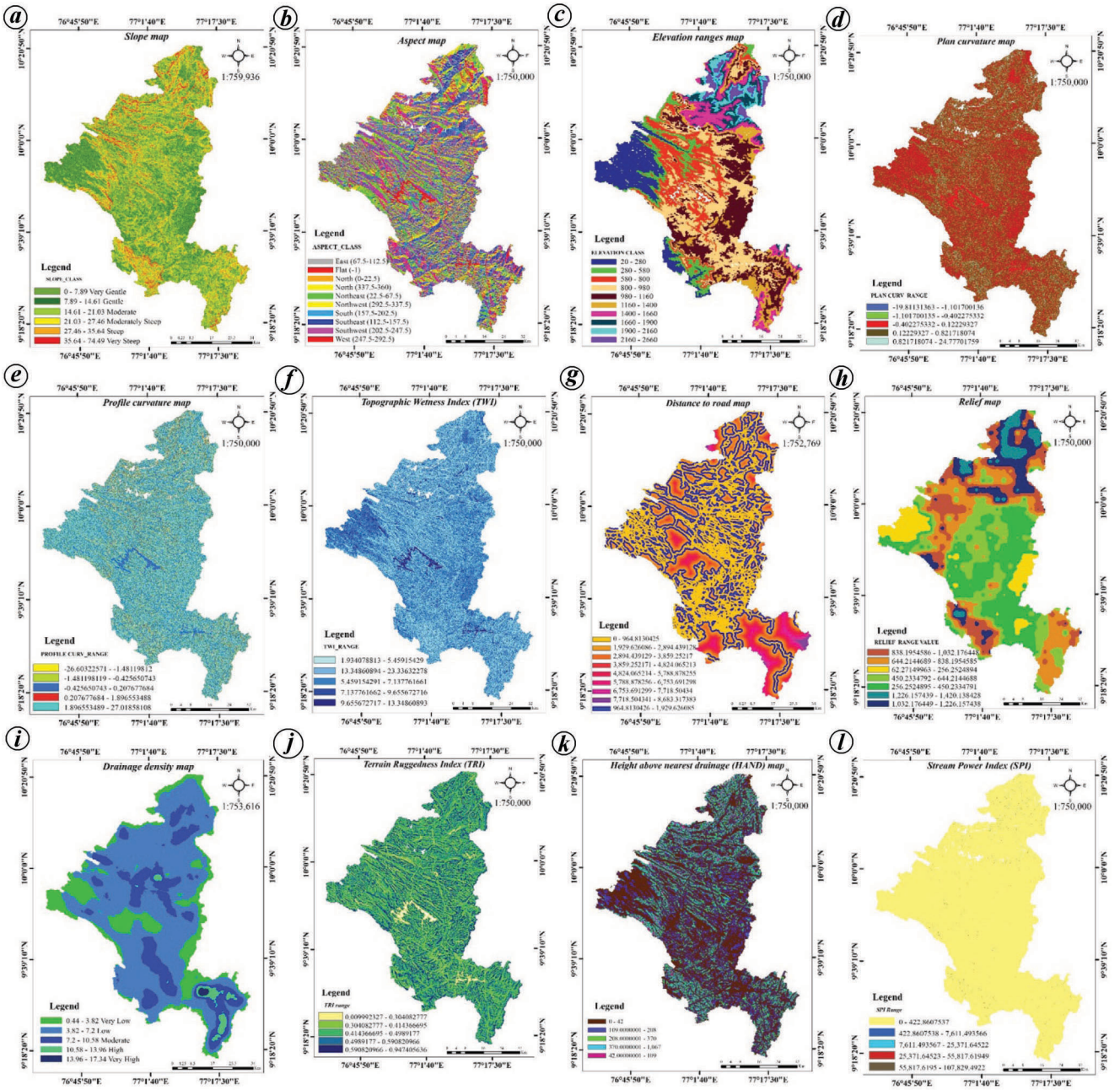

Figure 6. Feature classes corresponding to (***a***) slope, (***b***) aspect, (***c***) elevation, (***d***) plan curvature, (***e***) profile curvature, (***f***) topographic wetness index, (***g***) distance to road, (***h***) relative relief, (***i***) drainage density, (***j***) terrain ruggedness index (TRI), (***k***) height above near drainage (HAND) and (***l***) stream power index (SPI).

Assessment of landslides based on feature classification

The features for the entire Idukki district, Kerala, were derived from AW3D30 and mapped to the landslide inventory data to evaluate the presence of landslide points corresponding to different feature classes. A total of 14,430 locations were selected for assessment. Figure 7 *a–i* shows the number of locations under each class of all features for this assessment.

Figure 8 shows the percentage of landslides for different feature classes.

In Figure 8 *a*, the trend line shows that the higher the slope, the more likely a landslide occur. More than 80% of landslide points fall into different steep classes of the slope. The probable aspect classes where landslides have commonly occurred are north, south, northeast and southwest (Figure 8 *b*). The distribution of landslides across elevation categories, as depicted in Figure 8 *c*, indicates that higher elevations are predominantly associated with a

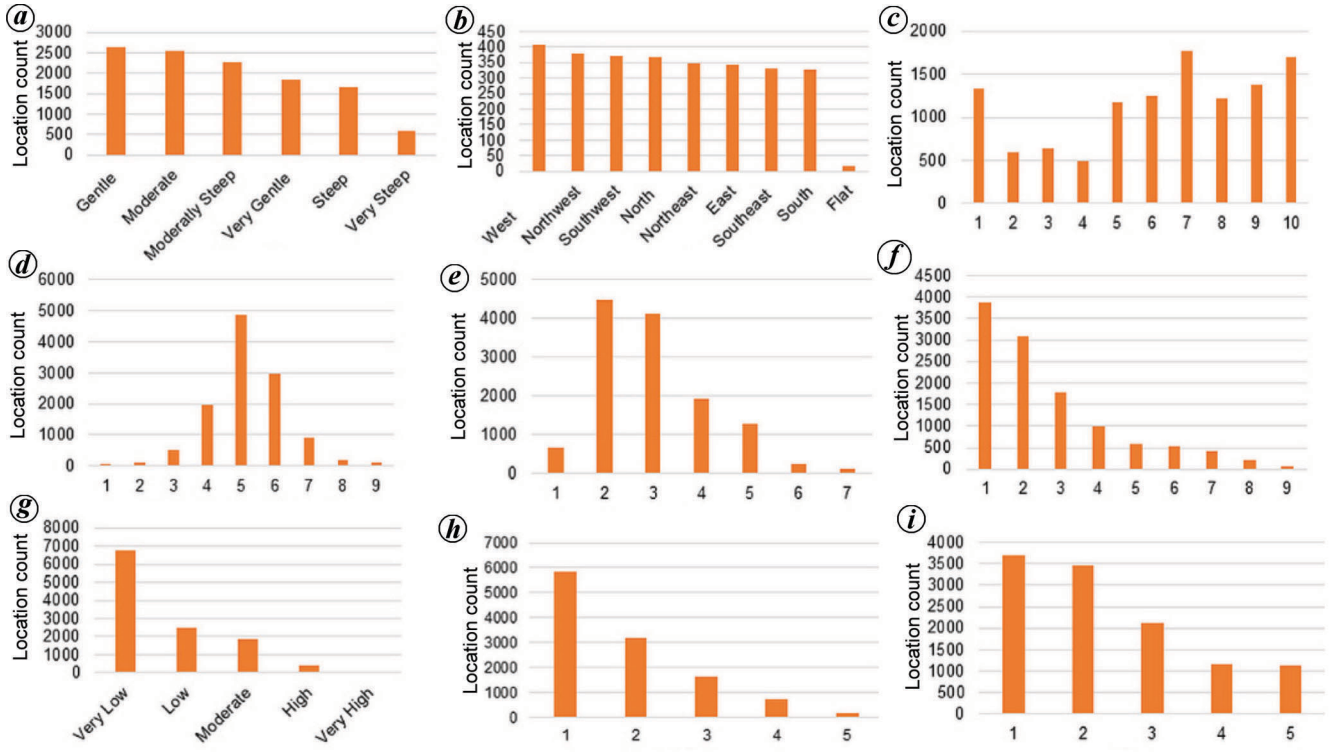

Figure 7. Number of locations under each class of all features: (***a***) slope, (***b***) aspect, (***c***) elevation, (***d***) profile curvature, (***e***) relative relief, (***f***) distance to road, (***g***) drainage density, (***h***) HAND and (***i***) SPI.

greater frequency of landslides. Here, most landslide points are in the elevation above 1900 m. The upward curve behaviour of profile and plan curvature directly impacts landslides (Figure 8 *d* and *e*) respectively. Among the nine classes of 'distance to road' features, those with relatively small distances closely resemble landslide points (Figure 8 *f*). Considering drainage density, most landslides are located at the head of the drainage classes with higher density (Figure 8 *g*). Higher wetness index values indicate wetter conditions, which can increase the likelihood of slope failure and landslides (Figure 8 *h*). The percentage of landslide points among the HAND classes shows that the risk of landslides increases as the vertical distance between a location and its nearest creek increases (Figure 8 *i*). More variation in elevation in a unit area relative to its local base level increases the risk of landslides (Figure 8 *j*). The percentage of landslides is more within the area having high relative relief. More than 50% of landslides fall into this category. Figure 8 *k* illustrates that elevated values within the higher SPI class are indicative of increased occurrences of landslides. These landslide influencing factors (LIFs) assessments can be used to determine the probability of landslide occurrences.

This study uses hydrogeological and geomorphological characteristics obtained from FABDEM that directly affect the susceptibility to landslides in the Idukki district, Kerala. The combination of features includes slope angles ranging from 27° to 75°, both north and south aspects, elevation between 1400 and 2660 m, a distance less than 1000 m from the roads and a high convex nature of profile curvature, ranging from 1.9 to 27. The variables impacting the incidence of landslides include relative relief above 6000 m, high drainage density and values exceeding 400 m for the HAND metric. Moreover, index values surpassing 9 for TWI, 0.5 for TRI and 5.0 for TPI have a direct effect on the occurrence of landslides within this geographical area.

Conclusion and future works

This study evaluates the accuracy of DEMs such as Cartosat-I, ASTER-GDEM SRTM-GL1, AW3D30 and FABDEM of 30 m resolution for the Idukki district, Kerala. The DEMs were mapped onto 264 spot heights selected randomly as reference points from the SOI topographical map and for different elevation categories. The performance of the various DEMs for all 264 points and elevation categories was evaluated using statistical measures. The RMSE of FABDEM was 41.79 m, which is low, followed by AW3D30, SRTM-GL1, ASTER-GDEM and Cartosat-I. With respect to elevation-wise accuracy, FABDEM was highly error-free, even in the high-elevation regions. Twelve geomorphological and hydrological features were derived from FABDEM and categorized using the ArcGIS Spatial Analyst tool. The distribution of feature classes and their proportion of surface existence were plotted. Landslides

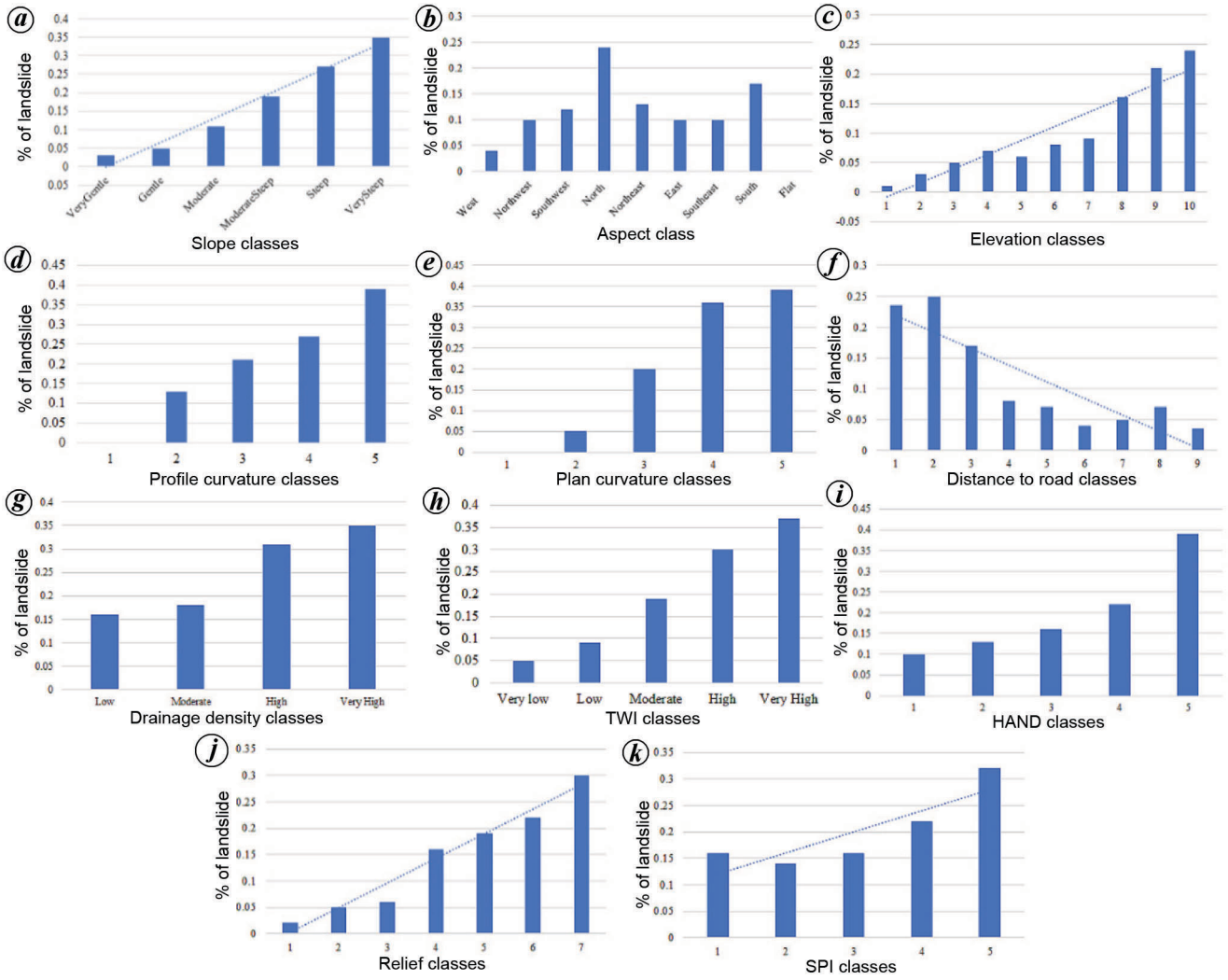

Figure 8. Percentage of slide points under (***a***) slope, (***b***) aspect, (***c***) elevation, (***d***) profile curvature, (***e***) plan curvature, (***f***) distance to road, (***g***) drainage density, (***h***) TWI, (***i***) HAND, (***j***) relative relief and (***k***) SPI.

were assessed by calculating their percentage existence on different feature classes. The study identified that a combination of features played a significant role in determining landslide occurrences in this region. The results reveal that the FABDEM model is the best for analysing landslide susceptibility mapping of the Idukki district, Kerala.

As a continuation of this work, a decision support system can be developed that utilizes the geomorphological and hydrogeological features derived from these open accesse 30 m resolution DEMs. The long-term aim is to assist the local Government bodies and the public in identifying the susceptibility of their location using publicly available DEM. This decision support system could aid in various applications related to topography and the environment, leveraging the available updated DEM data for the study region at any point.

1. Daya Sagar, B. S., Digital elevation models: an important source of data for geoscientists. *IEEE Geosci. Remote Sensing Mag.*, 2020, **8**(4), 138–142.
2. Coveney, S., Association of elevation error with surface type, vegetation class and data origin in discrete-returns airborne LiDAR. *Int. J. Geogr. Inf. Sci.*, 2013, **27**(3), 467–483.
3. Mesa-Mingorance, J. L. and Ariza-Lopez, F. J., Accuracy assessment of digital elevation models (DEMs): a critical review of practices of the past three decades. *Remote Sensing*, 2020, **12**(16), 2630.
4. Mohammed Al Balasmeh, O. I. and Karmaker, T., Accuracy assessment of the digital elevation model, digital terrain model (DTM) from aerial stereo pairs and contour maps for hydrological parameters. *Appl. Geomat. Civ. Eng.*, 2019, 461–470.
5. Mahesh, R., Sarunjith, J. K., Rajakumari, S., Muruganandam, R. and Ramesh, R., Quality assessment of open sourced digital elevation models in southeast coast of India. *Egypt. J. Remote Sensing Sci.*, 2021, **24**(3), 745–754.
6. Vaka, D. S., Kumar, V., Rao, Y. S. and Deo, R., Comparison of various DEMs for height accuracy assessment over different terrains of India. In IEEE International Geoscience and Remote Sensing Symposium, Yokohama, Japan, 14 November 2019; doi:10.1109/IGARSS.2019.8898492.
7. Mukherjeea, S., Joshi, P. K., Mukherjeea, S., Ghosh, A., Garg, R. D. and Mukhopadhyay, A., Evaluation of vertical accuracy of open source digital elevation model (DEM). *Int. J. Appl. Earth Obs. Geoinf.*, 2013, **21**, 205–217.

8. Rawat, K. S., Mishra, A. K., Sehgal, V. K., Ahmed, N. and Tripathi, V. K., Comparative evaluation of horizontal accuracy of elevations of selected ground control points from ASTER and SRTM DEM with respect to CARTOSAT-1 DEM: a case study of Shahjahanpur district, Uttar Pradesh, India. *Geocarto Int.*, 2013, **28**(5), 439–452.
9. Jain, A. O., Thaker, Chaurasia, P. and Singh, P., Vertical accuracy evaluation of SRTM-GL1, GDEM-V2, AW3D30 and CartoDEM-V3.1 of 30 m resolution with dual frequency GNSS for Lower Tapi Basin, India. *Geocarto Int.*, 2018, **33**, 1237–1256.
10. Patel, A., Katiyar, S. K. and Prasa, V., Performances evaluation of different open source DEMs using differential global positioning system (DGPS). *Egypt. J. Remote Sensing Space Sci.*, 2016, **19**, 7–16.
11. Mukherjee, S., Accuracy of Cartosat-1 DEM and its derived attribute at multiple scale representation. *J. Earth Syst. Sci*., 2015, **124**(3), 487–495.
12. Rastogi, G. and Agrawal, R., Bias corrections of CartoDEM using ICESat-GLAS data in hilly regions. *GISci. Remote Sensing*, 2015, **52**, 571–585.
13. Thomas, J., Joseph, S., Thrivikramji, K. P. and Arunkumar, K. S., Sensitivity of digital elevation models: the scenario from two tropical mountain river basins of the Western Ghats, India. *Geosci. Front*., 2014, **5**, 893–909.
14. Brocka, J., Schratza, P., Petschkoa, H., Muenchowa, J., Micuc, M. and Brenning, A., The performance of landslide susceptibility models critically depends on the quality of digital elevation models. *Geomat. Nat. Hazards Risk*, 2020, **11**(1), 1075–1092.
15. Jones, S., Kasthurba, A. K., Bhagyanathan, A. and Binoy, B. V., Landslide susceptibility investigation for Idukki district of Kerala using regression analysis and machine learning. *Arab. J. Geosci*., 2021, **14**, 838.
16. Jennifer, J. and Saravanan, S., Artificial neural network and sensitivity analysis in the landslide susceptibility mapping of Idukki district, India. *Geocarto Int*., 2021, **37**(10), 1–23.
17. Kieran, M. R., Hunt and Menon, A., The 2018 Kerala foods: a climate change perspective. *Climate Dyn*., 2020, **54**, 2433–2446.
18. Rao, B. S., Anil Kumar, G., Gopalakrishna, P. V. S. S. N., Srinivasulu, P. and Raghu Venkataraman, V., Evaluation of EGM 2008 with EGM96 and its utilization in topographical mapping projects. *J. Indian Soc. Remote Sensing*, 2021, **40**(2), 335–340.
19. Bertin, S., Jaud, M. and Delacourt, C., Assessing DEM quality and minimizing registration error in repeated geomorphic surveys with multi-temporal ground truths of invariant features: application to a long-term dataset of beach topography and nearshore bathymetry. *Earth Surf. Process. Landf.*, 2022, **47**, 2950–2971.
20. Krishnan, S., Sajikumar, N. and Sumam, K. S., DEM generation using Cartosat-I stereo data and its comparison with publically available DEM. *Proc. Technol.*, 2016, **24**, 295–302.
21. Muralikrishnan, S., Pillai, A., Narender, B., Reddy, S., Raghu Venkataraman, V. and Dadhwal, V. K., Validation of Indian national DEM from Cartosat-1 data. *J. Indian Soc. Remote Sensing*, 2013, **41**(1), 1–13.
22. Gesch, D., Oimoen, M., Danielson, J. and Meyer, D., Validation of the aster global digital elevation model version 3 over the conterminous United States. *Int. Arch. Photogramm., Remote Sensing Spat. Inf. Sci.*, 2016, **XLI-B4**, 143–148.
23. Foni, A. and Seal, D., Shuttle radar topography mission: an innovative approach to shuttle orbital control. *Acta Astronaut.*, 2004, **54**(8), 565–570.
24. Patel, P. P. and Sarkar, A., Terrain characterization using SRTM data. *J. Indian Soc. Remote Sensing*, 2010, **38**, 11–24.
25. Marsh, C. B., Harder, P. and Pomeroy, J. W., Validation of FABDEM, a global bare-earth elevation model, against UAV-lidar derived elevation in a complex forested mountain catchment. *Environ. Res. Commun.*, 2023, **5**(3), 1–19.
26. Tadono, T., Takaku, J., Tsutsui, K., Oda, F. and Nagai, H., Status of ALOS World 3D (AW3D) global DSM generation. In IEEE International Geoscience Remote Sensing Symposium, Milan, Italy, 2015.
27. Rawat, K. S., Sing, S. K., Singh, M. I. and Garg, B. L., Comparative evaluation of vertical accuracy of elevated points with ground control points from ASTER-DEM and SRTMDEM with respect to CARTOSAT-1DEM. *Remote Sensing Appl. Soc. Environ*., 2019, **13**, 289–297.
28. Cakir, L. and Konakoglu, B., The impact of data normalization on 2D coordinate transformation using GRNN. *Geod. Vestn*., 2019, **63**, 541–553.
29. Nath, R. R., Sharma, M. L., Goswami, A., Sweta, K. and Pareek, N., Landslide susceptibility zonation with special emphasis on tectonic features for occurrence of landslides in Lower Indian Himalaya. *J. Indian Soc. Remote Sensing*, 2021, **49**(5), 1221–1238.
30. Bopche, L. and Rege, P. P., Feature-based model for landslide susceptibility mapping usinga multi-parametric decision-making technique and the analytic hierarchy process. *Sådhanå*, 2021, **46**, 122.
31. Shirzadi, A., Bui, D. T., Pham, B. T. and Solaimani, K., Shallow landslide susceptibility assessment using a novel hybrid intelligence approach. *Environ. Earth Sci.*, 2017, **76**(2), 1–18.
32. Ghosh, T., Bhowmik, S., Jaiswal, P., Ghosh, S. and Kumar, D., Generating substantially complete landslide inventory using multiple data sources: a case study in Northwest Himalayas, India. *J. Geol. Soc. India*, 2020, **95**(1), 45–58.
33. Feby, B., Achu, A. L., Jimnisha, K., Ayisha, V. A. and Reghunath, R., Landslide susceptibility modelling using integrated evidential belief function based logistic regression method: a study from southern Western Ghats, India. *Remote Sensing Appl. Soc. Environ.*, 2020, **20**, 1–19.

Received 27 December 2022; revised accepted 13 June 2023

doi: 10.18520/cs/v125/i6/665-677